DENTAL MATERIALS 35 (2019) 883–892

Available online at www.sciencedirect.com

ScienceDirect

journal homepage: www.intl.elsevierhealth.com/journals/dema

In vitro biofilm formation on different ceramic biomaterial surfaces: Coating with two bactericidal glasses

A. Llama-Palacios[a], M.C. Sánchez[a], L.A. Díaz[b], B. Cabal[b], M. Suárez[b], J.S. Moya[b], R. Torrecillas[b], E. Figuero[a], M. Sanz[a], D. Herrera[a,*]

[a] ETEP (Etiology and Therapy of Periodontal Diseases) Research Group, University Complutense, Madrid, Spain
[b] Nanomaterials and Nanotechnology Research Center (CINN-CSIC), Universidad de Oviedo (UO), Principado de Asturias (PA), Avda. de la Vega 4-6, 33940 El Entrego, Spain

ARTICLE INFO

Article history:
Received 16 January 2019
Received in revised form
10 March 2019
Accepted 13 March 2019

Keywords:
Biofilm
CLSM
qPCR
Biocides
Nanocomposite
Hydroxyapatite
Bactericidal glass/glass-ceramic

ABSTRACT

Objectives. To compare biofilm formation on the surface of different ceramic biomaterials to be used in implant dentistry.

Methods. In vitro biofilm formation was investigated from mixtures of standard reference strains of *Streptococcus oralis*, *Veillonella parvula*, *Actinomyces naeslundii*, *Fusobacterium nucleatum*, *Aggregatibacter actinomycetemcomitans* and *Porphyromonas gingivalis*. Sterile ceramic calcium hydroxyapatite discs (HA) as control, sterile Al_2O_3/Ce-TZP nanocomposite sandblasted discs (material A1) and sterile Al_2O_3/Ce-TZP nanocomposite sandblasted discs and coated with two types of antimicrobial glasses (materials A2 and A3) were used. Biofilms were grown on the four surfaces and evaluated after 12, 24, 48 and 72 h of incubation. Biofilms were examined by confocal laser scanning microscopy (CLSM). In addition, counts of live bacterial cells of the target species *A. actinomycetemcomitans*, *F. nucleatum* and *P. gingivalis* were calculated by quantitative polymerase chain reaction (qPCR) combined with propidium monoazide (PMA). For data analysis, bacterial counts were compared with a multivariate general lineal model.

Results. Using CLSM, cell vitality decreased in A2 and A3. With qPCR-PMA, significant differences in vitality were observed for*A. actinomycetemcomitans* in A3 after 48 and 72 h of incubation. With respect to the development of the biofilms, a significant increase in counts on HA and materials A1 and A2 was observed for *A. actinomycetemcomitans* and *F. nucleatum*. Conversely, for *P. gingivalis*, no differences were found for HA and materials A1 and A2.

Significance. Differences in biofilm formation were detected among the different tested materials. The ceramic material A3 has an effect on the vitality of *A. actinomycetemcomitans* growing in an *in vitro* biofilm model.

* *Corresponding author at*: Faculty of Odontology, Plaza Ramón y Cajal s/n — (Ciudad Universitaria), 28040 Madrid, Spain.
E-mail address: davidher@ucm.es (D. Herrera).

https://doi.org/10.1016/j.dental.2019.03.003

1. Introduction

Oral diseases are the most prevalent human diseases and continue to affect the majority of the world population [1]. Among them, dental caries and periodontal diseases, including gingivitis and periodontitis [2] are caused by bacteria organized as biofilms adhered to dental surfaces. In the oral cavity, microorganisms grow adhered to the different available surfaces (tooth surfaces, dental restorations, implants, oral mucosa, etc.) [3] forming three-dimensional biofilms, where these bacterial communities are supported by an extracellular matrix of polysaccharides. The surface characteristics on which these biofilms develop have an important influence on the types of bacterial communities involved, on the ratio of binding of bacteria to the surface, on the bacterial phenotype or the expression of virulence factors and/or extracellular polysaccharides [4–7].

Similar to tooth surfaces, dental implant surfaces develop complex biofilms and the interaction of these biofilms with the local host response has important pathogenic influence in the development of peri-implant diseases [8–12]. Experimental studies have demonstrated that implant micro-surface topography significantly influence bacterial adhesion and development of peri-implantitis [13,14]. Consequently, there is a strong interest in the development of new materials demonstrating bacterial adherence inhibition and antibacterial properties [6,10,15–20].

Inert bioceramics, such as Alumina Toughened Zirconia (ATZ) and Zirconia Toughened Alumina (ZTA), have been successfully used as components for orthopaedic and dental applications, due to their biocompatibility, their mechanical properties (i.e. flexural strength and fracture toughness for orthopaedics) and aesthetics (dental restorations) [21–24]. For dental applications it is also fundamental the ability of these surfaces to osseointegrate, which is heavily dependent on their composition and micro-surface roughness [25]. It is for this reason that these bioceramics need to be treated, either with sandblasting or with the use of other nanocomposite molecules that enhance bone cell adhesion and differentiation [26,27].

A new ceramic nanocomposite biomaterial (Al_2O_3/Ce-TZP) has been developed as potential implant surface able to osseointegrate, but with lesser biofilm accumulation. Furthermore, non-toxic biocidal materials (G3-GC and 35ZnO-G glasses) have been added to this biomaterial and have been tested for their antimicrobial effect on planktonic and biofilm cultures of different bacterial and fungal species [16,18,20,28–32], but there are no studies evaluating their antibacterial activity in complex biofilm models. It is therefore, the purpose of this *in vitro* investigation to evaluate the antibacterial activity in an *in vitro* complex biofilm model of different surfaces of Al_2O_3/Ce-TZP nanocomposite sandblasted with white corundum coated with two types of antimicrobial glasses, 35ZnO-G and G3-GC glass biocides.

2. Materials and methods

2.1. Bacterial strains and culture conditions

Standard reference strains of *Streptococcus oralis* CECT 907 T, *Veillonella parvula* NCTC 11810, *Actinomyces naeslundii* ATCC 19039, *Fusobacterium nucleatum* DMSZ 20482, *Aggregatibacter actinomycetemcomitans* DSMZ 8324 and *Porphyromonas gingivalis* ATCC 33277 were selected. These bacteria were grown on blood agar plates (Blood Agar Oxoid No 2; Oxoid, Basingstoke, UK), supplemented with 5% (v/v) sterile horse blood (Oxoid), 5.0 mg mL^{-1} hemin (Sigma, St. Louis, MO, USA) and 1.0 mg mL^{-1} menadione (Merck, Darmstadt, Germany) in anaerobic conditions (10% H_2, 10% CO_2, and balance N_2) at 37 °C for 24–72 h.

2.2. Material processing and microstructural characterization

The Al_2O_3/Ce-TZP nanocomposite was made using the following materials: Ce-TZP (10 mol% CeO_2) from Daichi Kigenso Kagaku Kogyo Co., LTD (Osaka, Japan) with an average particle size of 35 nm (d_{50}) and a specific surface area of 15 $m^2\,g^{-1}$; α-Al_2O_3 powder (TM DAR, Taimei Chemicals Co., LTD, Tokyo, Japan) with a specific surface area of 14,6 $m^2\,g^{-1}$ and an average particle size of 150 nm; aluminum chloride (Sigma); 99,97% absolute ethanol (Panreac Química SLU, Barcelona, Spain) and 99.9% 2-propanol (Panreac). In addition, the following chemical precursors were also used: (i) aluminum chloride (Sigma), (ii) zirconium IV-propoxide (70% solution in 1-propanol) (Sigma), and (iii) 99.97% absolute ethanol (Panreac). By using a colloidal processing route based on co-doping of starting alumina and 10 mol% Ce-TZP nano powders, it was possible to obtain fully dense Zirconia Toughened Alumina (ZTA) nanocomposites after sintering in air [33].

These powders were cold isostically pressed at 300 MPa into cylindrical rods of 50 mm in length and 9 mm in diameter. After surface grinding and firing at 1475 °C in a laboratory furnace (Termolab. Águeda, Portugal) for one hour, disc shaped specimens with a diameter of 7 mm and a thickness of 1.8 mm were prepared by cutting and polishing using micropolishes (Struers, Ballerup, Denmark) of 9, 3 and 1 μm. On these polished surfaces the sandblasting was carried out. Samples were sandblasted for 60 s using white corundum particles (particle size less 90 μm or $d_{50} < 90$ μm) using ASTURSINTER® sandblaster machine (Oviedo, Spain). The disc was placed perpendicular to the nozzle of the air abrasion unit and located 10 mm away. The air pressure was set to 0.4 bar.

Two antimicrobial glasses were selected: one is a soda-lime glass from SiO_2–Na_2O–Al_2O_3–CaO–B_2O_3 system labeled as G3-GC [18], and the other one belongs to the B_2O_3–SiO_2–Na_2O–Al_2O_3–ZnO system labeled as 35ZnO-G [16]. Coatings using these antimicrobial glasses by screen-printing technology were done. A polymer ink, based on a mixture of epoxy and glass powder was prepared for the glass layer

Table 1 – The selected conditions and names of different surface processes applied to Al_2O_3/Ce-TZP nanocomposite are shown (sandblasting and coating nomenclature).

Samples	Composition	Coating
A1	Al_2O_3/Ce-TZP nanocomposite sandblasted and uncoated	None
A2	Al_2O_3/Ce-TZP nanocomposite sandblasted and coated with an antimicrobial soda–lime-glass powder (named G3-GC) (chemical composition (wt. %): 41.6 SiO_2, 20.0 Na_2O, 19.5 CaO, 10.1 Al_2O_3, 6.4 B_2O_3, 0.21 MgO and 0.61 K_2O (Nanoker Research, S.L. Spain) [18]	G3 glass biocide
A3	Al_2O_3/Ce-TZP nanocomposite sandblasted and coated with a zinc-containing glass. Its chemical composition (wt. %): 19.39 SiO_2; 34.24 B_2O_3; 5.55 Na_2O; 5.13 Al_2O_3 and 34.73 ZnO. This glass was labelled as 35ZnO-G [16]	35ZnO glass biocide

A1, A2, and A3 were all sandblasted for 60 s with white corundum (particle size <90 μm).

Table 2 – Volumetric fractions of monoclinic phase zirconia present on different sandblasted and aged surfaced.

Surface treatment (ADD)	Monoclinic phase content (%$V_{m\ total}$)
(1) Al_2O_3/Ce-TZP as-sintered	3.80 ± 3
(2) Al_2O_3/Ce-TZP as-sintered and ageing for 5 h	2.10 ± 3
(3) Al_2O_3/Ce-TZP as-sintered and sandblasted surface with white corundum <90 μm, 60 s	24.73 ± 3
(4) Al_2O_3/Ce-TZP as-sintered, sandblasted surface with white corundum <90 μm, 60 s, and aged for 5 h.	27.00 ± 3

(1), (2), (3) and (4) corresponding to the number of surface as indicated in the text.

screen-printing. This layer was deposited on the sandblasting surfaces. Both green coatings were thermally treated at 750 °C/1 h and the thickness of the glass film once sintered was about 40 μm verify by the use of a Field Emission Scanning Electron Microscopy (FESEM) (FEI Quanta FEG 650, Thermo Fisher Scientific, Oregon, USA). Sterile calcium hydroxyapatite discs (Clarkson Chromatography Products, Williamsport, PA, USA) were used as control (HA). Table 1 shows a summary of the different surface materials that were used for biofilm testing.

2.2.1. *Morphology and surface roughness*

To characterize the surface topography of the raw materials and the different surfaces prepared in this study, microscopic observations were also studied by FESEM. Surface roughness of the specimens was analyzed using a surface roughness tester (MicroTest MT4002, MicroTest, Madrid, Spain). Six areas about 6 mm^2 were measured for each specimen according to ISO 4287-1997 [34]. The evaluated profile (Ra) as an arithmetic mean deviation of these six measurements was calculated.

2.2.2. *X-ray diffraction analysis*

The amount of transformation (monoclinic volume content), which was induced by sandblasting, was determined by X-ray diffraction (XRD) with the D8 Discover (Bruker Corporation, Massachusetts, USA) using the method of Toraya et al. [35]. In the nanocomposite, the resistance against low temperature degradation (LDT) was studied with an autoclave (Tuttnauer 2540 EL; Tuttnauer, NY, USA) following the ISO 13356 2008 [36]. This technique is an accelerated test at intermediate temperatures (100–300 °C) for extrapolating an estimate the transformation rate and the product lifetime [37]. It is widely demonstrated that extensive transformation to the m-polymorph causes a deterioration of the mechanical properties, especially the bending strength [38,39]. Table 2 shows as the as-sintered surfaces and aged for different time durations to monitor the change in volume fraction Al_2O_3/Ce-TZP nanocomposite were further sandblasted.

2.3. *Biofilm development*

Biofilms were grown on the four surfaces as previously described by Sánchez et al. [40]. In brief, pure cultures of each bacterium were grown anaerobically in a protein-rich medium containing brain–heart infusion (BHI) (Becton, Dickinson and Company, Franklin Lakes, NJ, USA) supplemented with 2.5 $g\,L^{-1}$ mucin (Oxoid), 1.0 $g\,L^{-1}$ yeast extract (Oxoid), 0.1 $g\,L^{-1}$ cysteine (Sigma), 2.0 $g\,L^{-1}$ sodium bicarbonate (Merck), 5.0 $mg\,mL^{-1}$ hemin (Sigma), 1.0 $mg\,mL^{-1}$ menadione (Merck) and 0.25% (v/v) glutamic acid (Sigma). The bacterial growth was harvested at mid-exponential phase (measured by spectrophotometry), and a mixed bacteria suspension in modified BHI medium, containing 10^3 colony-forming units (CFU) mL^{-1} for *S. oralis*, 10^5 CFU mL^{-1} for *V. parvula* and *A. naeslundii*, and 10^6 CFU mL^{-1} for *F. nucleatum, A. actinomycetemcomitans* and *P. gingivalis,* was prepared. Sterile discs were placed in the wells of a 24-well tissue culture plate (Greiner Bio-one, Frickenhausen, Germany). Each well was inoculated with 1.5 mL mixed bacteria suspension prepared and incubated in anaerobic conditions (10% H_2, 10% CO_2, and balance N_2) at 37 °C for 12, 24, 48 and 72 h. Plates containing only culture medium were also incubated to check for sterility. These experiments were repeated twice on three different days using fresh bacterial cultures (n = 6).

2.4. *Analysis of biofilms by Confocal Laser Scanning Microscopy (CLSM)*

Before CLSM analysis, the discs were sequentially rinsed in 2 mL of sterile saline phosphate buffer (PBS) (immersion time per rinse, 10 s) three times, to remove non-adherent bacteria. With the use of a non-invasive confocal fixed-stage Ix83

Table 3 – Primers and probes used for quantification of genomic DNA from the target bacteria. Primers and probes were targeted against 16S rRNA gene.

Bacteria	Sequence (5´–3´)	Length (bp)	Reference
Aa			
Forward	GAACCTTACCTACTCTTGACATCCGAA	80	[54]
Reverse	TGCAGCACCTGTCTCAAAGC		
Probe	6FAM-AGAACTCAGAGATGGGTTTGTGCCTTAGGG-TAMRA		
Fn			
Forward	GGATTTATTGGGCGTAAAGC	162	[54]
Reverse	GGCATTCCTACAAATATCTACGAA		
Probe	6FAM-CTCTACACTTGTAGTTCCG-TAMRA		
Pg			
Forward	GCGCTCAACGTTCAGCC	67	[55]
Reverse	CACGAATTCCGCCTGC		
Probe	6FAM-CACTGAACTCAAGCCCGGCAGTTTCAA-TAMRA		

Bp: Base pairs. *Aa*, *A. actinomycetemcomitans*; *Fn*, *F. nucleatum*; *Pg*, *P. gingivalis*.

Olympus inverted microscope coupled to an Olympus FV1200 confocal system with ×63 water-immersion lenses (Olympus; Shinjuku, Tokyo, Japan) the fully hydrated biofilms were studied. Biofilms were previously stained with the LIVE/DEAD® BacLight™ Bacterial Viability Kit solution (Molecular Probes B. V., Leiden, The Netherlands). This staining uses two fluorochromes (SYTO9 green-fluorescent nucleic acid stain and propidium iodide red-flurescent nucleic acid), at 1:1 ration and 9 ± 1 min of staining time at the corresponding wave lengths (Syto9: 515–530 nm; PI: >600 nm), which makes possible to differentiate between viable and dead bacteria. This analysis was carried out at the Fluorescence Cytometry and Microscopy Centre at the Universidad Complutense de Madrid.

2.5. *DNA isolation and quantitative Polymerase Chain Reaction (qPCR)*

Before the DNA isolation, the discs were sequentially rinsed in 2 mL of sterile PBS (immersion time per rinse, 10 s) three times to remove non-adherent bacteria. Then the disks were treated with Propidium monoazide (PMA) (Biotium Inc., Hayward, CA, USA) to analyse the live cells present in the biofilm as described in previously [41]. Briefly, biofilms were disrupted by vortex for 2 min in 1 mL of PBS. PMA was added to sample tubes containing 250 μL of the disaggregated biofilm cells, at a final concentration of 100 μM. Following an incubation period of 10 min at 4 °C in the dark, the samples were subjected to light-exposure for 20 min, using a 550 W halogen light source, placed 20 cm above the samples. During this exposure, the sample tubes were laid horizontally on ice to avoid excessive heating. After PMA photo-induced DNA cross-linking, the cells were centrifuged at 9000 × *g* for 3 min prior to DNA isolation. To control for any possible influence of the experimental process on bacterial viability, the same procedure (incubation at 4 °C and exposure to light source), but without the exposure to PMA, was used as negative control.

The DNA was then isolated from all samples using a commercial kit (ATP Genomic DNA Mini Kit®; ATP biotech, Taipei, Taiwan), following manufacturer's instructions. Primers and probes targeted against 16S *rRNA* gene were synthesized by Life Technologies Invitrogen (Carlsbad, CA, USA) and Applied Biosystems (Carlsbad, CA, USA). Sequences are shown in Table 3. The qPCR amplification method was used in a total reaction mixture volume of 20 μL. The reaction mixtures contained 10 μL of 2x master mixture (LC 480 Probes Master; Roche Diagnostic GmbH; Mannheim, Germany), optimal concentrations of primers and probe (300, 300 and 100 nM for *A. actinomycetemcomitans*; 300, 300 and 300 nM, for *P. gingivalis* and 600, 600 and 300 nM for *F. nucleatum*), and 5 μL of DNA from samples. The negative control was 5 μL of sterile water [no template control (NTC)] (Water PCR grade, Roche). The samples were subjected to an initial amplification cycle of 95 °C for 10 min, followed by 40 cycles at 95 °C for 15 s and 60 °C for 1 min. Analyses were performed with a LightCycler® 480 II thermocycler (Roche). The plates used in the study were FramStar 480 of natural frame and white wells (4titude; The North Barn; Damphurst Lane, UK), sealed by QPCR Adhesive Clear Seals (4titude).

Each DNA sample was analysed in duplicate. Quantification cycle (Cq) values, previously known as cycle threshold (Ct) values, describing the PCR cycle number at which fluorescence rises above the baseline, were determined using the provided software package (LC 480 Software 1.5; Roche). Quantification of viable and total cells by qPCR was based on standard curves, following a protocol previously described [41]. The correlation between Cq values and CFU/mL was automatically generated through the software (LC 480 Software 1.5; Roche).

All assays were developed with a linear quantitative detection range established by the slope range of 3.3–3.6 cycles/log decade, $r^2 > 0.997$ and an efficiency range of 1.9–2.0. Measures to avoid carryover DNA were established. In spite of this, when NTC was detectable, the limit of detection was established on the last value of the standard curve that holds five cycles of difference with NTC.

2.6. *Data analysis*

These assays were repeated six times for each biomaterial (HA, A1, A2, A3), and outcomes were measured at four times (12, 24, 48 and 72 h), evaluating three target species (*A. actinomycetemcomitans*, *F. nucleatum*, *P. gingivalis*).

Means [colony forming units (CFU)/mL] for the counts of a given bacterial species, over a certain material and at a determined time were calculated. Shapiro–Wilk goodness-of-

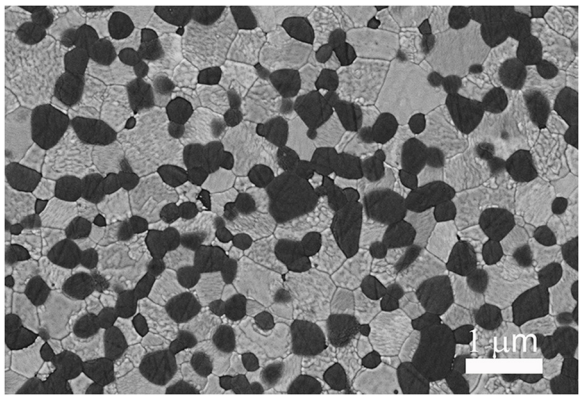

Fig. 1 – FESEM image of the polished surface of the Al_2O_3/Ce-TZP nanocomposite. Matrix is composed of Ce-TZP crystals (grey color) and the darkness crystals are alumina.

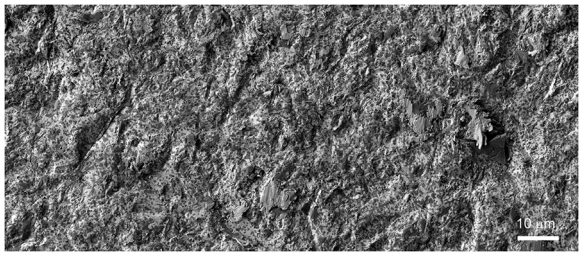

Fig. 2 – FESEM image of the sandblasted surface of the nanocomposite with white corundum raw material.

fit tests and graphical distribution of data were used to assess normality. Data as means and 95% confidence intervals (CI) were expressed.

A multivariate general model with Bonferroni's correction was used to compare the numbers of live cells on the tested biomaterials (n = 4) at each time (n = 4) for each independent bacterial species.

Results were considered statistically significant when $p < 0.05$. A software package (IBM SPSS Statistics 21.0; IBM Corporation, Armonk, NY, USA) was used for all data analysis.

3. Results

3.1. *Ceramic biomaterials characterization*

Fig. 1 shows the microstructure of the Al_2O_3/Ce-TZP nanocomposite. It is composed of a matrix of Ce-TZP grains (of size 400–500 nm) and a homogeneously distributed a second phase of alumina crystals (of average size of 250 nm). Fig. 2, shows the Al_2O_3/Ce-TZP nanocomposite surface after sandblasting by white corundum.

Roughness values (Ra) of the ZTA nanocomposite surfaces with and without sandblasting were 0.465 ± 0.06 and 0.031 ± 0.10, respectively.

The volumetric fraction of the monoclinic phase was measured on: (1) as-sintered surfaces, (2) as-sintered surfaces after sandblasting process, and (3) as-sintered surfaces after sandblasting and its ageing process. As can be seen in Table 2, the Al_2O_3/Ce-TZP nanocomposite does not present spontaneous phase transformation on their surface after sintering and any ageing process (surfaces 1 and 2). However, sandblasting processes leads to the transformation, under tension, of a part of the tetragonal zirconia to monoclinic zirconia (surfaces 3 and 4). This transformation process is reversible and, in every case, a thermal treatment to 1200 °C for 15 min was carried out. This heat treatment transformed the totally of the monoclinic zirconia back to its initial tetragonal state [23,42].

In Figs. 3 and 4, the coatings of G3-GC and 35ZnO-G glasses deposited on the sandblasting Al_2O_3/Ce-TZP nanocomposite substrates are shown. As observed in Fig. 3A, the deposited glass G3-GC shows two crystalline phases: nepheline and combeite [32]. It can be seen "platelets" or "narrow rectangular features" of willemite crystals, precipitate inside the annealing glass (Fig. 4A).

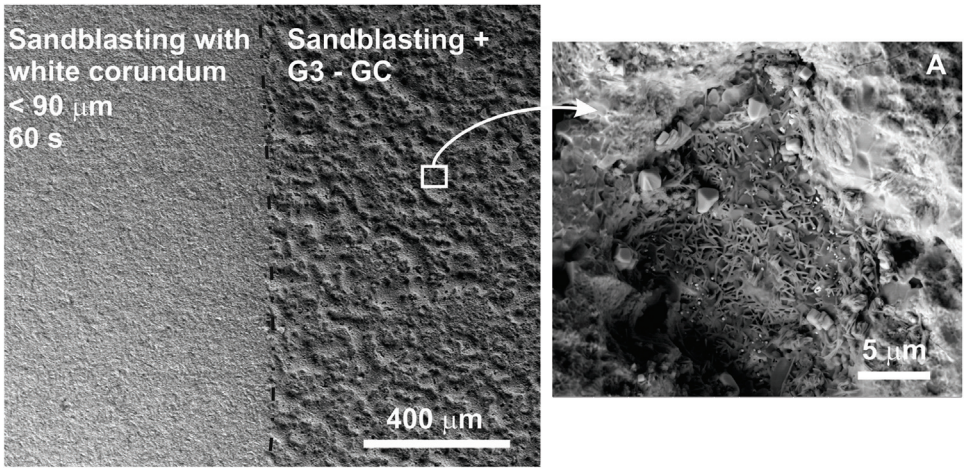

Fig. 3 – Backscattered electron image (FESEM) of Al_2O_3/Ce-TZP nanocomposite (sample A2) sandblasted with white corundum only (<90 μm, 60 s) (left) and sandblasted and coated with antibacterial glass G3-GC (right). A) Image of the framework of nepheline crystals. The combeite crystals are much smaller (arrows) (<50 nm).

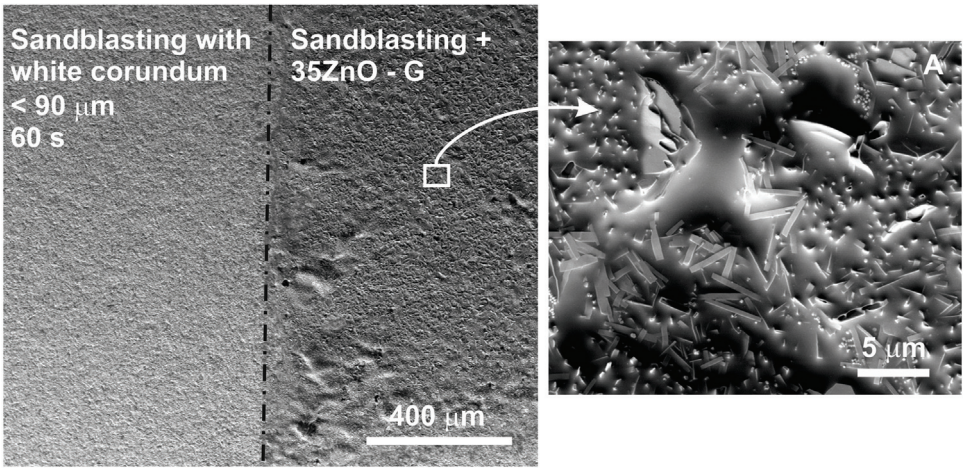

Fig. 4 – Backscattered electron image (FESEM) of Al_2O_3/Ce-TZP nanocomposite (sample A3) sandblasted with white corundum and coated with antibacterial glass 35ZnO-G. A) Crystallization of willemite (Zn_2SiO_4) platelets.

3.2. *Biofilm structure analyzed by CLSM*

Fig. 5 depicts the CLSM generated topographic maps using several fields of vision of the biofilm growth and maturation on the different biomaterial surfaces (HA, A1, A2, A3) at the different time periods (12, 24, 48 and 72 h of incubation).

After 12 h of incubation, biofilms consisted mostly of a large bacterial community attached to the surface of the different materials, arranged either as single cells or as short streptococcal chains. On the surface of material A2, a red background was observed, probably due to the affinity of propidium iodide for this material. At this time of incubation, most cells were alive (in green), although in the material A3 some dead cells (in red) already begin appear (Fig. 5).

After 24 h, the typical biofilm "towers" or bacterial cell stacks are clearly formed, especially on HA and material A2, although HA-disks demonstrated more live cells. On material A2, the red background was still observed, although less intense because the biofilm was developing over the whole surface of the discs (Fig. 5).

After 48 h, more viable cells were observed on HA, as compared to the materials coated with the biocide glasses (A2 and A3) (Fig. 5). Similar results were observed at 72 h, although differences were more evident, especially for material A3 with more evidence of dead cells (Fig. 5).

3.3. *Quantitative analysis of biofilms by qPCR*

Table 4 shows the counts (CFU/biofilm) of live cells for the three target bacterial species analyzed on the four studied surfaces, at the different incubation times.

For *A. actinomycetemcomitans*, significant increases in counts were observed on HA disks from 12 to 72 h (72 h versus 12 h and 24 h; $p < 0.001$; 72 h versus 48 h; $p = 0.002$). The materials A1 and A2 showed a similar pattern, with live cells demonstrating a statistically significant increase until 48 h, but no further growth was detected from 48 to 72 h (material A1: 48 h versus 12 h, $p = 0.003$; 48 h versus 24 h, $p = 0.049$; material A2: 48 h versus 12 h, $p = 0.031$). In the material A3, however, no statistically significant differences were observed among the studied time periods.

For *F. nucleatum*, similarly, the number of cells increased significantly from 12 h to 48 h of incubation in both HA and material A2 ($p < 0.05$). For material A1, there was a statistically significant increase from 12 h to 48 h (48 h versus 12 h, $p = 0.008$), but then it decreased significantly at 72 h ($p = 0.031$). For material A3, there were no statistically significant differences among the studied time periods.

For *P. gingivalis*, no statistically significant differences were observed for HA and materials A1 and A2. For material A3, there was a significant increase in the number of counts for up to 72 h (72 h versus 12 h, 24 h and 48 h, $p = 0.000$).

When comparing the differences in bacterial counts among the tested materials at the different incubation times, no significant differences were found for *F. nucleatum* at any tested time, although material A2 was the one with the highest number of viable cells of this bacterium. For *A. actinomycetemcomitans*, only after 48 h, material A3 had a significant lower biofilm formation when compared to materials A2 ($p = 0.002$) and A1 ($p = 0.001$). After 72 h, statistically significant differences were detected between material A3 and HA ($p < 0.000$) and A2 ($p = 0.008$), and also between HA and material A1 ($p = 0.026$), being HA the material with a biofilm with higher content of live cells. For *P. gingivalis*, only after 72 h, statistically significant differences were observed between material A3 and HA ($p = 0.038$), and materials A1 ($p = 0.002$) and A2 ($p = 0.015$), and the material A3 had the biofilm with the highest counts of this bacterium.

4. Discussion

The results from this *in vitro* investigation have shown that the added bactericidal glasses on the tested biomaterials (35ZnO-G) [16,30] and (G3-GC) [18,29] exerted an antimicrobial effect on the development of a complex biofilm model when compared with a control surface (HA) (Fig. 5). Specifically, 35ZnO-G glasses had a significant impact on bacterial growth for *A. actinomycetemcomitans* at 48 and 72 h and for *P. gingivalis* at 72 h of

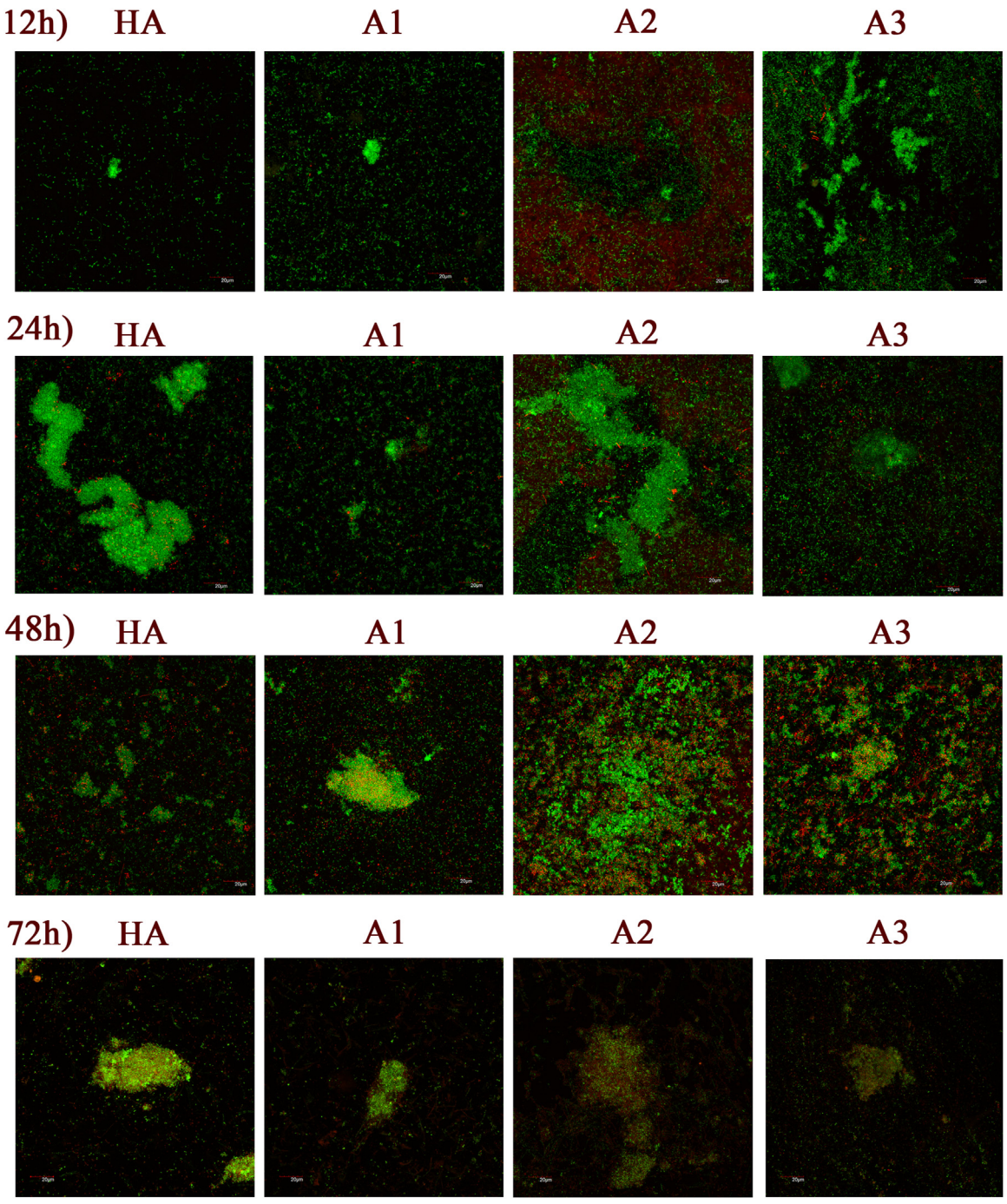

Fig. 5 – Confocal micrographs representing a 2D maximum projection of biofilms after 12 h, 24 h, 48 h and 72 h incubated on (HA) hydroxyapatite; (A1) sample A1; (A2) sample A2; (A3) sample A3. LIVE/DEAD® BacLight™ Bacterial Viability Kit was used to assess the vitality of cells. (For interpretation of the references to colour in the text, the reader is referred to the web version of this article).

incubation; resulting in lesser counts of *A. actinomycetemcomitans* and *F. nucleatum* when compared with the other tested biomaterials.

The complex biofilm model used in this investigation has been validated in previous studies [5,40,41,43] and it is relatively easy to standardize for reproducible laboratory simulation of the oral condition. The selected bacterial species are representative from bacteria associated with periodontal health and disease and included initial colonizers as *S. oralis*, intermediate colonizers, belonging to the genus *Actinomyces* or *Veillonella*, and late colonizers including *A. actinomycetemcomitans* and *P. gingivalis*, which are species strongly associated to both periodontitis and peri-implantitis [44–46]. With regards, to the incubation times, 72 h is the time that the biofilm has reached maturity in this *in vitro* model, while after 96 h of incu-

Table 4 – Number of viable bacteria in the *in vitro* multi-species biofilm (colony forming units, CFU/mL). Data is expressed as means and 95% confidence intervals (CI).

Bacteria	Time	Viable CFU/mL [mean (95% CI)]			
		HA	A1	A2	A3
Aa	12 h	5.21×10^5 (-7.21×10^5; 1.76×10^6)	3.79×10^5 (-8.63×10^5; 1.62×10^6)	8.10×10^5 (-4.32×10^5; 2.05×10^6)	1.68×10^5 (-1.07×10^6; 1.41×10^6)
	24 h	1.22×10^6 (-1.90×10^4; 2.46×10^6)	1.23×10^6 (-1.08×10^4; 2.47×10^6)	1.63×10^6 (3.85×10^5; 2.87×10^6)	3.29×10^5 (-9.13×10^5; 1.57×10^6)
	48 h	1.71×10^6 (4.71×10^5; 2.95×10^6)	3.63×10^6 (2.38×10^6; 4.87×10^6)	3.35×10^6 (2.11×10^6; 4.59×10^6)	6.07×10^4 (-1.20×10^6; 1.30×10^6)
	72 h	5.09×10^6 (3.85×10^6; 6.34×10^6)	**2.51×10^6** (1.26×10^6; 3.75×10^6)	3.13×10^6 (1.88×10^6; 4.37×10^6)	**1.80×10^5** (-1.06×10^6; 1.42×10^6)
Fn	12 h	8.3×10^4 (-1.53×10^6; 1.70×10^6)	6.19×10^4 (-1.55×10^6; 1.68×10^6)	1.69×10^5 (-1.45×10^6; 1.78×10^6)	7.81×10^4 (-1.54×10^6; 1.69×10^6)
	24 h	1.09×10^6 (-5.31×10^5; 2.70×10^6)	7.59×10^5 (-8.58×10^5; 2.37×10^6)	1.64×10^6 (2.18×10^4; 3.25×10^6)	1.05×10^6 (-5.66×10^5; 2.67×10^6)
	48 h	3.31×10^6 (1.70×10^6; 4.93×10^6)	3.87×10^6 (2.25×10^6; 5.48×10^6)	3.50×10^6 (1.88×10^6; 5.11×10^6)	1.20×10^6 (-4.13×10^5; 2.82×10^6)
	72 h	1.18×10^6 (-4.37×10^5; 2.80×10^6)	5.59×10^5 (-1.06×10^6; 2.17×10^6)	1.20×10^6 (-4.13×10^5; 2.82×10^6)	5.18×10^5 (-1.10×10^6; 2.13×10^6)
Pg	12 h	5.87×10^3 (-1.32×10^6; 1.33×10^6)	3.97×10^3 (-1.32×10^6; 1.33×10^6)	6.71×10^3 (-1.32×10^6; 1.33×10^6)	5.82×10^3 (-1.32×10^6; 1.33×10^6)
	24 h	7.66×10^3 (-1.32×10^6; 1.33×10^6)	1.11×10^4 (-1.31×10^6; 1.33×10^6)	1.76×10^4 (-1.31×10^6; 1.34×10^6)	1.52×10^4 (-1.31×10^6; 1.34×10^6)
	48 h	6.58×10^4 (-1.26×10^6; 1.39×10^6)	8.99×10^4 (-1.23×10^6; 1.41×10^6)	2.66×10^5 (-1.06×10^6; 1.59×10^6)	6.60×10^4 (-1.26×10^6; 1.39×10^6)
	72 h	1.49×10^6 (1.68×10^5; 2.81×10^6)	5.28×10^5 (-7.95×10^5; 1.85×10^6)	1.20×10^6 (-1.25×10^5; 2.52×10^6)	**4.12×10^6** (2.80×10^6; 5.45×10^6)

In bold, statistically significant differences ($p < 0.05$) when compared with hydroxyapatite (HA) (control).
HA: hydroxyapatite; A1: material A1; A2: material A2; A3: material A3.

bation, the mortality of bacterial cells significantly increase [5,40].

Using CLSM, biomaterials coated with biocidal glasses demonstrated lesser number of live cells after 48 h and 72 h of incubation, when compared with the control surface (HA) and these differences were more evident for the material A3 after 72 h (Fig. 5). These differences between the biomaterials could be due to differences in the antimicrobial mode of action, since the glass enriched with CaO (G3-GC glass biocide) (material A2) needs a close contact with the target cells, acting by membrane depolarization of the microorganisms attached to the glass surface [18,29]; while for the 35ZnO-G glass (material A3), the antimicrobial activity can be attributed to the release of Zn^{2+} [16,30], what may imply easier diffusion and access to all bacterial cells present in the biofilm. The present results are in agreement with those published in Lopez-Piriz et al. [31], where the extend of bacterial adhesion on the glasses (G3-GC and 35ZnO-G) coating implant abutments decreased significantly, and only few microorganisms were detected growing on these coating. With material A1, minor differences with HA were observed, since the roughness produced by white corundum sandblasting may have favored the development of the biofilm, since according to the Altbrektsson and Wennerberg classification [47], samples sandblasted with white corundum present a surface roughness "smooth" ($Ra < 0.5\ \mu m$).

Both glasses G3-GC and 35ZnO-G are highly durable. They act as a delivery system providing sustained release of the ions. Elementary chemical mechanisms responsible for dissolution of these glasses are similar to the one observed for bioactive glasses (silicate glasses); they include hydratation, exchange of protonated species (H^+, H_3O^+) with alkali or earth alkali ions (interdiffusion), and the hydrolysis of the covalent bonds, followed by a possible configuration of the glass network into another rearrangement. The process of Zn^{2+} lixiviation from the glass network of 35ZnO-G has been studied by X-ray photoelectron spectroscopy (XPS) [30]. From these results we can state that the process of lixiviation of Zn^{2+} from the glass network is similar to the one observed in silicate glasses, where Na^+ is lixiviated to the media first and the fraction of Zn that acts as modifiers ($\tilde{2}/3$) is lixiviated in second place. After the subsequent collapse of the outer surface glass layer (about 200–300 nm thick layer) the dissolution process starts again. This glass is an excellent dispenser of Zn^{2+} to the media for a very long period of time, in the range of years. Something similar happens with the glass-ceramic G3-GC. Calcium is contained in both combeite crystals and the residual glassy phase of the glass-ceramic [48]. Dissolution of parent glass is similar to the one observed for bioactive glasses [49]. On the other hand, combeite is a complex structure constituted by piling of 6-fold silica tetrahedral rings. Sodium atoms are placed in the center of these rings. Alternated calcium and sodium atoms are located in the open space between the rings columns of sodium. Then, these calcium ions, as a consequence of its light bonding, can be easily exchanged by H^+ (or H_3O^+) ions from the solution in a similar way than in the original glass structure [48]. As a way of example, in a previous work, the chemical stability and the durability of G3-GC coated titanium alloy (Ti–6Al–4V) were evaluated by immersion in artificial saliva at 30 °C during 3 months. In the conditions in which the experiment was carried out, around 40% of the

coating was dissolved after 3 months of treatment. In this particular case the durability of this antimicrobial coating was expected to be more than 4 months [50].

Using qPCR for determining the specific bacterial counts within the biofilm, similar trends were found. The rise in the counts for the three tested bacterial species (*A. actinomycetemcomitans, F. nucleatum* and *P. gingivalis*) up to 48 h were similar on the control surface HA and materials A1 and A2, while with the biomaterial A3 (coated with 35ZnO-G), counts of *A. actinomycetemcomitans* and *F. nucleatum* did not increase with time. When comparing among the tested surfaces, this biomaterial A3 showed significant lesser counts for *A. actinomycetemcomitans* at 48 and 72 h of incubation, and for *P. gingivalis* at 72 h of incubation. These differences can be attributed to the activity of the zinc oxide (ZnO) and the increased diffusion of the Zn^{2+} ion with demonstrated antibacterial activity [16,30]. The mechanism of the biocidal action of ZnO involves membrane disrupting and generation of reactive oxygen species (ROS) leading to bacterial death [51–53]. In addition, the selectivity in the antimicrobial effect over different bacterial species could be explained by the different penetrability of ZnO into the bacterial membranes. Conversely, since biomaterial A2 has as main antimicrobial effect of the CaO (calcium oxide) membrane depolarization those microorganisms attached to the glass surface, this effect will only affect those initial primary colonizers, but not those bacteria forming the core of the biofilm [18].

Within the limitations of this *in vitro* model, it can be concluded that differences in biofilm formation were detected among the different tested biomaterials: the ceramic material A3, with ZnO enriched glass biocide, demonstrated a clear antibacterial effect at different times of incubation, when compared with the control surface and the other tested biomaterial surfaces, what may represent a good candidate for further testing in dental implant applications.

Acknowledgments

This work was supported by the Spanish Ministry of Economy and Competitiveness (MINECO) under the project MAT2012-38645. A.L.-P. and M.C.S. received funding from Extraordinary Chair of DENTAID-UCM. We acknowledge the technical assistance of Alfonso Cortés from the Centre of Microscopy and Cytometry from the University Complutense, Madrid. We thank Raquelina del Rosario Pianeta Alviz, Honorato Vidal and Giacomo Piacentini for their technical assistance during their work for the *Trabajo Fin de Master*.

REFERENCES

[1] Kassebaum NJ, Bernabe E, Dahiya M, Bhandari B, Murray CJ, Marcenes W. Global burden of severe periodontitis in 1990–2010: a systematic review and meta-regression. J Dent Res 2014;93:1045–53.

[2] Sanz M, Beighton D, Curtis MA, Cury JA, Dige I, Dommisch H, et al. Role of microbial biofilms in the maintenance of oral health and in the development of dental caries and periodontal diseases. Consensus report of group 1 of the Joint EFP/ORCA workshop on the boundaries between caries and periodontal disease. J Clin Periodontol 2017;44(Suppl 18):S5–11.

[3] Whittaker CJ, Klier CM, Kolenbrander PE. Mechanisms of adhesion by oral bacteria. Annu Rev Microbiol 1996;50:513–52.

[4] Rizzello L, Sorce B, Sabella S, Vecchio G, Galeone A, Brunetti V, et al. Impact of nanoscale topography on genomics and proteomics of adherent bacteria. ACS Nano 2011;5:1865–76.

[5] Sanchez MC, Llama-Palacios A, Fernandez E, Figuero E, Marin MJ, Leon R, et al. An *in vitro* biofilm model associated to dental implants: structural and quantitative analysis of in vitro biofilm formation on different dental implant surfaces. Dent Mater 2014;30:1161–71.

[6] Cabal B, Cafini F, Esteban-Tejeda L, Alou L, Bartolome JF, Sevillano D, et al. Inhibitory effect on in vitro *Streptococcus oralis* biofilm of a soda-lime glass containing silver nanoparticles coating on titanium alloy. PLoS One 2012;7:e42393.

[7] Teughels W, Van Assche N, Sliepen I, Quirynen M. Effect of material characteristics and/or surface topography on biofilm development. Clin Oral Implants Res 2006;17(Suppl 2):68–81.

[8] Lee A, Wang HL. Biofilm related to dental implants. Implant Dent 2010;19:387–93.

[9] Lang NP, Berglundh T, Working Group 4 of Seventh European Workshop on P. Periimplant diseases: where are we now? Consensus of the Seventh European Workshop on Periodontology. J Clin Periodontol 2011;38(Suppl 11):178–81.

[10] Busscher HJ, Rinastiti M, Siswomihardjo W, van der Mei HC. Biofilm formation on dental restorative and implant materials. J Dent Res 2010;89:657–65.

[11] Sanz-Martin I, Sanz-Sanchez I, Carrillo de Albornoz A, Figuero E, Sanz M. Effects of modified abutment characteristics on peri-implant soft tissue health: a systematic review and meta-analysis. Clin Oral Implants Res 2018;29:118–29.

[12] Nascimento C, Pita MS, Santos Ede S, Monesi N, Pedrazzi V, Albuquerque Jr RF, et al. Microbiome of titanium and zirconia dental implants abutments. Dent Mater 2016;32:93–101.

[13] Albouy JP, Abrahamsson I, Persson LG, Berglundh T. Implant surface characteristics influence the outcome of treatment of peri-implantitis: an experimental study in dogs. J Clin Periodontol 2011;38:58–64.

[14] Albouy JP, Abrahamsson I, Berglundh T. Spontaneous progression of experimental peri-implantitis at implants with different surface characteristics: an experimental study in dogs. J Clin Periodontol 2012;39:182–7.

[15] Esteban-Tejeda L, Diaz LA, Prado C, Cabal B, Torrecillas R, Moya JS. Calcium and zinc containing bactericidal glass coatings for biomedical metallic substrates. Int J Mol Sci 2014;15:13030–44.

[16] Esteban-Tejeda L, Prado C, Cabal B, Sanz J, Torrecillas R, Moya JS. Antibacterial and antifungal activity of ZnO containing glasses. PLoS One 2015;10:e0132709.

[17] Lopez-Esteban S, Bartolome JF, Diaz LA, Esteban-Tejeda L, Prado C, et al. Mechanical performance of a biocompatible biocide soda-lime glass-ceramic. J Mech Behav Biomed Mater 2014;34:302–12.

[18] Moya JS, Esteban-Tejeda L, Pecharroman C, Mello-Castanho SRH, da Silva AC, et al. Glass powders with a high content of calcium oxide: a step towards a ğreenüniversal biocide. Adv Eng Mater 2011;13:B256–60.

[19] Esteban-Tejeda L, Díaz LA, Cabal B, Prado C, Lopez-Piriz R, Torrecillas R, et al. Biocide glass–ceramic coating on titanium alloy and zirconium oxide for dental applications. Mater Lett 2013;111:4.

[20] Esteban-Tejeda L, Cabal B, Torrecillas R, Prado C, Fernandez-Garcia E, Lopez-Piriz R, et al. Antimicrobial activity of submicron glass fibres incorporated as a filler to a dental sealer. Biomed Mater 2016;11:045014.
[21] Torrecillas R, Moya JS, Diaz LA, Bartolome JF, Fernandez A, Lopez-Esteban S. Nanotechnology in joint replacement. Wiley Interdiscip Rev Nanomed Nanobiotechnol 2009;1:540–52.
[22] Chevalier J, Taddei P, Gremillard L, Deville S, Fantozzi G, Bartolome JF, et al. Reliability assessment in advanced nanocomposite materials for orthopaedic applications. J Mech Behav Biomed Mater 2011;4:303–14.
[23] Benzaid R, Chevalier J, Saadaoui M, Fantozzi G, Nawa M, Diaz LA, et al. Fracture toughness, strength and slow crack growth in a ceria stabilized zirconia-alumina nanocomposite for medical applications. Biomaterials 2008;29:3636–41.
[24] Lopez-Piriz R, Fernandez A, Goyos-Ball L, Rivera S, Diaz LA, Fernandez-Dominguez M, et al. Performance of a new Al_2O_3/Ce-TZP ceramic nanocomposite dental implant: a pilot study in dogs. Materials (Basel) 2017;10.
[25] Le Guehennec L, Soueidan A, Layrolle P, Amouriq Y. Surface treatments of titanium dental implants for rapid osseointegration. Dent Mater 2007;23:844–54.
[26] Hayes JS, Khan IM, Archer CW, Richards RG. The role of surface microtopography in the modulation of osteoblast differentiation. Eur Cell Mater 2010;20:98–108.
[27] Bartolome JF, Moya JS, Couceiro R, Gutierrez-Gonzalez CF, Guitian F, Martinez-Insua A. In vitro and in vivo evaluation of a new zirconia/niobium biocermet for hard tissue replacement. Biomaterials 2016;76:313–20.
[28] Cabal B, Alou L, Cafini F, Couceiro R, Sevillano D, Esteban-Tejeda L, et al. A new biocompatible and antibacterial phosphate free glass-ceramic for medical applications. Sci Rep 2014;4:5440.
[29] Moya JS, Cabal B, Sanz J, da Silva AC, Mello-Castanho S, Torrecillas R, et al. Mechanism of calcium lixiviation in soda-lime glasses with a strong biocide activity. Mater Lett 2012;70:3.
[30] Esteban-Tejeda L, Palomares FJ, Cabal B, Lopez-Piriz R, Fernandez A, Sevillano D, et al. Effect of the medium composition on the Zn^{2+} lixiviation and the antifouling properties of a glass with a high ZnO content. Materials (Basel) 2017;10.
[31] Lopez-Piriz R, Sola-Linares E, Rodriguez-Portugal M, Malpica B, Diaz-Guemes I, Enciso S, et al. Evaluation in a dog model of three antimicrobial glassy coatings: prevention of bone loss around implants and microbial assessments. PLoS One 2015;10:e0140374.
[32] Lopez-Piriz R, Diaz LA, Cabal B, Fernandez A, Suarez M, Diaz R, et al. Prevention of periodontitis by the addition of a bactericidal particulate glass/glass-ceramic to a dental resin: a pilot study in dogs. Coatings 2018;8:12.
[33] Rivera S, Diaz LA, Fernandez A, Torrecillas R, Moya JS. Reinforcement mechanisms in alumina toughened zirconia nanocomposites with different stabilizing agents. 37th International Conference and Expo on Advanced Ceramics and Composites (ICACĆ13) 2013.
[34] 4287:1997 I. Geometrical Product Specifications (GPS)–surface texture: profile method—terms, definitions and surface texture parameters. 1997.
[35] Toraya H, Yoshimura M, Somiya M. Calibration curve for quantitative analysis of the monoclinic tetragonal ZrO_2 system by X-rays diffraction. J Am Ceram Soc 1984;67:3.
[36] 13356:2008 I. Implants for surgery-ceramic materials based on yttria-stabilized tetragonal zirconia (Y-TZP). 2008.
[37] Lughi V, Sergo V. Low temperature degradation -aging- of zirconia: a critical review of the relevant aspects in dentistry. Dent Mater 2010;26:807–20.
[38] Deville S, Chevalier J, Dauvergne C, Fantozzi G, Bartolome JF, Moya JS, et al. Microstructural investigation of the aging behavior of (3Y-TZP)-Al_2O_3 composites. J Am Ceram Soc 2005;88:7.
[39] Deville S, Chevalier J, Fantozzi G, Bartolome JB, Requena J, Moya JS, et al. Low-temperature ageing of zirconia-toughened alumina ceramics and its implication in biomedical implants. J Eur Ceram Soc 2003;23:7.
[40] Sanchez MC, Llama-Palacios A, Blanc V, Leon R, Herrera D, Sanz M. Structure, viability and bacterial kinetics of an *in vitro* biofilm model using six bacteria from the subgingival microbiota. J Periodontal Res Suppl 2011;46:252–60.
[41] Sanchez MC, Marin MJ, Figuero E, Llama-Palacios A, Leon R, Blanc V, et al. Quantitative real-time PCR combined with propidium monoazide for the selective quantification of viable periodontal pathogens in an in vitro subgingival biofilm model. J Periodontal Res Suppl 2014;49:20–8.
[42] Tanaka K, Tamura J, Kawanabe K, Nawa M, Uchida M, Kokubo T, et al. Phase stability after aging and its influence on pin-on-disk wear properties of Ce-TZP/Al_2O_3 nanocomposite and conventional Y-TZP. J Biomed Mater Res A 2003;67:200–7.
[43] Sanchez MC, Fernandez E, Llama-Palacios A, Figuero E, Herrera D, Sanz M. Response to antiseptic agents of periodontal pathogens in in vitro biofilms on titanium and zirconium surfaces. Dent Mater 2017;33:446–53.
[44] Quirynen M, De Soete M, van Steenberghe D. Infectious risks for oral implants: a review of the literature. Clin Oral Implants Res 2002;13:1–19.
[45] Listgarten MA. Microorganisms and dental implants. J Periodontol 1999;70:220–2.
[46] Listgarten MA, Lai CH. Comparative microbiological characteristics of failing implants and periodontally diseased teeth. J Periodontol 1999;70:431–7.
[47] Albrektsson T, Wennerberg A. Oral implant surfaces: part 1—review focusing on topographic and chemical properties of different surfaces and in vivo responses to them. Int J Prosthodont 2004;17:536–43.
[48] Cabal B, Alou L, Cafini F, Couceiro R, Sevillano D, Esteban-Tejeda L, et al. A new biocompatible and antibacterial phosphate free glass-ceramic for medical applications. Sci Rep 2014;4.
[49] Moya JS, Cabal B, Sanz J, Da Silva AC, Mello-Castanho S, Torrecillas R, et al. Mechanism of calcium lixiviation in soda-lime glasses with a strong biocide activity. Mater Lett 2012;70:113–5.
[50] Esteban-Tejeda L, Diaz LA, Cabal B, Prado C, Lopez-Piriz R, Torrecillas R, et al. Biocide glass-ceramic coating on titanium alloy and zirconium oxide for dental applications. Mater Lett 2013;111:59–62.
[51] Padmavathy N, Vijayaraghavan R. Enhanced bioactivity of ZnO nanoparticles-an antimicrobial study. Sci Technol Adv Mater 2008;9:035004.
[52] Reddy KM, Feris K, Bell J, Wingett DG, Hanley C, Punnoose A. Selective toxicity of zinc oxide nanoparticles to prokaryotic and eukaryotic systems. Appl Phys Lett 2007;90:2139021–3.
[53] Xie Y, He Y, Irwin PL, Jin T, Shi X. Antibacterial activity and mechanism of action of zinc oxide nanoparticles against *Campylobacter jejuni*. Appl Environ Microbiol 2011;77:2325–31.
[54] Boutaga K, van Winkelhoff AJ, Vandenbroucke-Grauls CM, Savelkoul PH. Periodontal pathogens: a quantitative comparison of anaerobic culture and real-time PCR. FEMS Immunol Med Microbiol 2005;45:191–9.
[55] Boutaga K, van Winkelhoff AJ, Vandenbroucke-Grauls CM, Savelkoul PH. Comparison of real-time PCR and culture for detection of *Porphyromonas gingivalis* in subgingival plaque samples. J Clin Microbiol 2003;41:4950–4.